FAR APPROACH OPTICAL NAVIGATION AND COMET PHOTOMETRY FOR THE ROSETTA MISSION

Francesco Castellini[(1,2)], David Antal-Wokes[(1,3)], Ramon Pardo de Santayana[(1,4)] and Klaas Vantournhout[(1,5)]

[(1)] *ESOC, Robert-Bosch-Straße 5, 64293 Darmstadt Germany*
[(2)] *Telespazio VEGA Deutschland GmbH, Francesco.Castellini@esa.int*
[(3)] *SciSys Deutschland GmbH, David.Wokes@esa.int*
[(4)] *GMV GmbH, Ramon.Pardo@esa.int*
[(5)] *CGI Deutschland Ltd. & Co., Klaas.Vantournhout@esa.int*

Abstract: *This paper presents the optical navigation activities carried out by the Rosetta Flight Dynamics team before reaching 67P/Churyumov-Gerasimenko in August 2014, and the analysis of the comet photometric properties performed for operational purposes both before and after the spacecraft arrival at the comet. Details are provided for the developed methods and algorithms, including quantitative results from operational data, covering first the optical detection of the comet with the on-board cameras, the far approach optical measurements for orbit determination purposes, the light-curve analysis for rotational period estimation, and the developed photometric models for comet 67P, which allowed proper selection of the camera exposure times and gradual transition from manual to automatic landmarks processing.*

Keywords: *Comet optical detection, optical data reduction, light-curve analysis, photometry.*

1. Introduction

On January 20th, 2014, the European Space Agency's Rosetta spacecraft woke up after 2.55 years of deep space hibernation. After a re-commissioning period and a series of braking manoeuvers from May to July, it rendezvoused with comet 67P/Churyumov-Gerasimenko in August and successfully delivered the lander Philae to the surface in November. Throughout all these phases, Rosetta relied heavily on optical navigation, first for on-board detection of the comet and far-approach navigation, then for landmark-based proximity operations. Separate papers provide the overview of the Rosetta mission's comet phase from the Flight Dynamics perspective [1] and of the landmark-based optical processing [2], [3]. This paper focuses on the optical navigation activities carried out before reaching the comet in August and on an analysis of the photometric properties of the comet and the related operational consequences, such as selecting camera exposure times.
Rosetta's optical navigation uses two dedicated navigation cameras (navcams), complemented for special operations and redundancy purposes by its science cameras [4], the Osiris Narrow Angle Camera (NAC) and Wide Angle Camera (WAC). The first optical operation after hibernation exit was the early detection from the on-board cameras of comet 67P. The NAC was used for this purpose due to its better sensitivity with respect to the Navcams (limiting magnitude of 15 against 11). Details are given in the paper regarding the developed algorithms and their application, leading to the successful detection at the first attempted slot on March 24th.
As soon as the comet was acquired, far approach optical navigation was started with the purpose of providing as input for the orbit determination process the direction in azimuth and elevation of the centroid of the comet. Development of the tools for this far approach navigation had already

been carried out for Rosetta's fly-bys of asteroids Steins and Lutetia, and is described in details in [5]. For Rosetta, approach images were taken initially with the Osiris NAC, transitioning to Navcam when the comet was bright enough in May. The paper describes the three distinct phases that can be distinguished in the far approach optical navigation activities: initially, the comet was sufficiently faint to detect enough stars to accurately fit the camera attitude, hence correcting for thermal effects and attitude controller error, resulting in errors well below 1 pixel; from July 3rd, at approximately 44,000 km from the comet with a magnitude around 2, separate images with longer exposure had to be taken for the stars, averaging the camera alignment and leading to about 1 pixel accuracy; finally, from July 24th and until the beginning of landmark-based navigation on August 6th, centroiding errors for the extended comet - which was larger than 15 pixels at less than 3500 km - exceeded the attitude errors, thus making star-images useless.
In parallel to the retrieval of optical imagery for the far approach phase, a photometric lightcurve was obtained over 12 days. This data was used to obtain a precise estimation of the comet's rotational period, later used as input for the attitude reconstruction of the comet. From July 11th until the 31st, photometric data was obtained every 2.5 seconds with the Navcam in the coined "asteroid-tracking mode". The rotational period of the comet was obtained through a combination of periodic folding and $\chi 2$-fitting of distance-corrected periodic Fourier components. Results of this analysis are presented in the paper, showing the peculiar light-curve properties of double-lobed 67P with a first estimated period of 12.425 ± 0.013 hours.
Finally, an analysis of the basic photometric properties of 67P/Churyumov-Gerasimenko was carried out by the Flight Dynamics team throughout both approach and comet characterization phases of the Rosetta mission. Three models were developed and tuned to the characteristics of 67P, one for the point-source comet during approach and two for the comet as extended object during proximity navigation. These had the main purposes of enabling the appropriate selection of camera exposure times and of estimating the values of the photometric parameters necessary for the generation of the maplets for automatic image processing (See [3] and [6]). The use of different models allowed coping with different requirements in different phases of the mission, initially ensuring robustness to the yet unknown features of the comet, and later on enabling a much reduced workload through nearly automated optical processing.

All details of the developed methods are presented in the following sections, including quantitative results from operational data, covering first the comet optical detection, then the far approach optical measurements and light-curve analysis, and finally the photometric models for comet 67P.

2. Optical detection of comet 67P Churyumov-Gerasimenko

After Rosetta woke-up from hibernation and re-commissioning of both spacecraft platform and payloads was concluded, acquisition of the comet by the on-board imaging instruments was the first mission objective during the approach phase. Comet detection was to be attempted already from the end of March 2014, when estimates of 67P's visual magnitude were between 12 and 15, with the goal of introducing the target direction information in the optimization of the first braking maneuver and, therefore, save precious propellant. This was only going to be possible with the NAC from the Osiris science instrument, capable of detecting faint objects up to magnitude 15. Detection with Navcams was foreseen as backup strategy in case of contingencies with the NAC, as the lower sensitivity allowed only identifying objects as bright as magnitude

11. As it turned out, the Osiris NAC has been working flawlessly for the past year and a half, and the comet was therefore successfully detected at the first attempted slot on March 24th. It was not until the beginning of May that it was finally visible also in Navcam images, with optical measurements gradually transitioning from NAC to Navcam until the beginning of June.

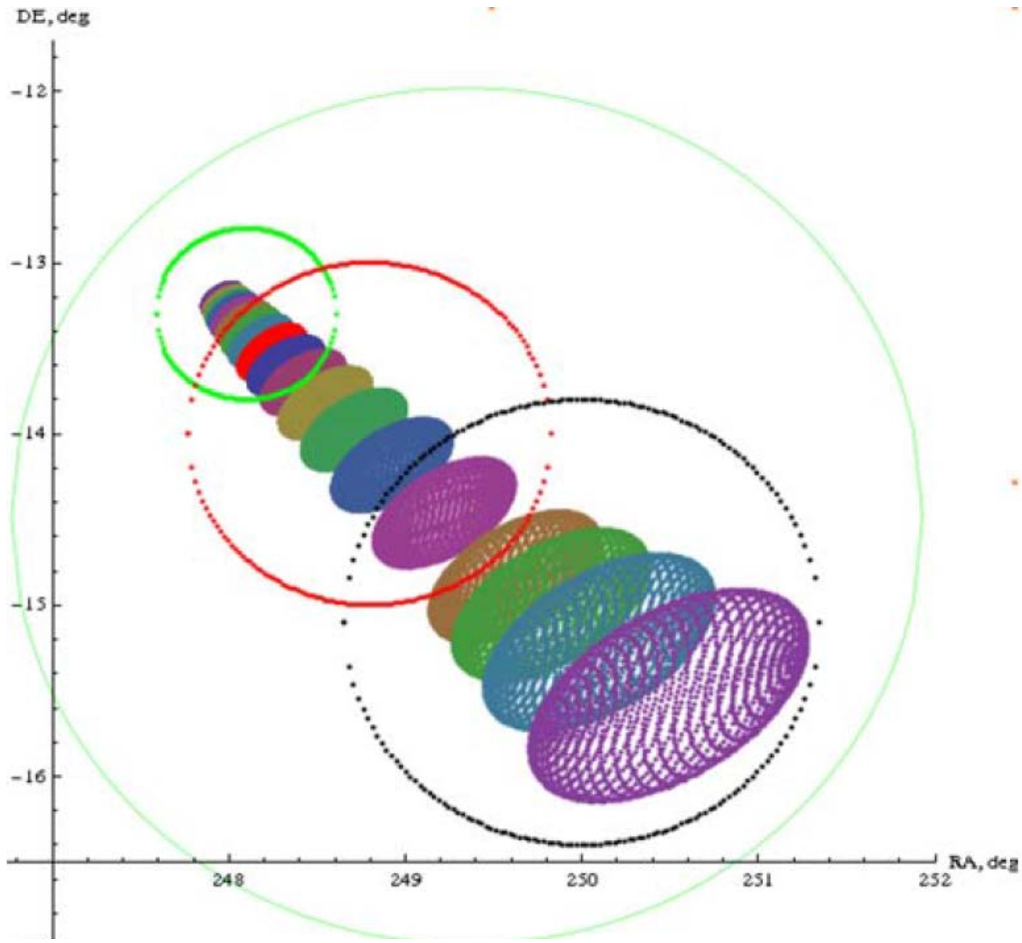

Figure 1. Pre-detection uncertainty ellipsoids for the comet inertial direction. Dotted circles: search cones for April, beginning and end of May. Solid circle: Navcam 5 deg FoV.

Figure 1 summarizes the detection options, showing the expected position and uncertainty of the comet in inertial J2000 Right Ascension (RA) and Declination (DE), as known in mid-March. The uncertainty ellipsoids grew larger from the end of March (top left) to the end of May (bottom right) due to the closer distance, hence three detection periods were identified. During the last week of March and April, the NAC was pointed towards the search area indicated by the green dotted line, with 0.5 deg of half-cone angle. In the first half of May, pointing was going to be the red area, almost filling up the 2.2 deg Field of View (FoV) of the NAC. Finally, the back-up Navcam slot is represented by the black dotted line. For each period, two imaging slots per week were foreseen, each including 5 images with different integration times. Although in the end not necessary, this approach had been designed to be robust to both camera hardware issues and unexpected comet behavior, such as much lower luminosity or much different position with respect to the predictions.

To succeed in the optical detection already with a comet magnitude of ~15, an ad-hoc image processing software was developed with the purpose of automatically matching the acquired light sources with a much larger star catalogue than the one previously used for asteroid fly-bys, ideally leaving only a handful of candidates to be manually screened. This was the PPMXL catalogue [7], containing positions, proper motions, 2MASS and optical photometry of 900 million stars and galaxies, complete down to about magnitude 20 full-sky.

The developed automatic process starts with the generation of clusters from the images, i.e. blocks of adjacent pixels above a given threshold which may represent a real celestial object, a Single Event Upset (SEU) or a CCD artifact. The brighter of these clusters are then matched against the Hipparcos/Tycho catalogue, obtaining an estimate of the camera inertial attitude which is more accurate with respect to the available telemetry. The large number of clusters (5000-20000 for NAC images and 50000-70000 for Navcam images, depending on the threshold) is then reduced by filtering those outside the search cone area, those recognized as SEUs due to small size or large stretching, and those with too low signal with respect to the expected comet magnitude. As the conversion from CCD signal to visual magnitude, calibrated with sun-like stars, introduces a large error, a significant margin has to be kept to avoid the risk of discarding 67P (e.g. mag 16 instead of the worst-case expected 15). The remaining clusters are then matched against the stars in the PPMXL catalogue. After filtering the stars in the catalogue for search area and magnitude, their inertial direction is corrected for stellar aberration and converted to expected pixel positions through the reconstructed camera attitude and calibrated optical models.

Two types of cluster-star matching are implemented: a Single Star Matching (SSM) algorithm, which checks if a given cluster is within a given threshold from any star, usually set to 1 pixel (~1 mdeg for NAC, ~5 mdeg for Navcam), and a more complex Multiple Stars Matching (MSM) method. This was introduced for cases when two or more stars merge in a single cluster, as shown for instance in Figure 2. Here, the single stars are too far away to be detected with the SSM threshold of ~1 pixel, hence a larger threshold of ~2 pixels is defined, and the expected signal of all stars within this larger search cone is combined to estimate the centroid, which can then be matched within 1 pixel to the cluster on the image.

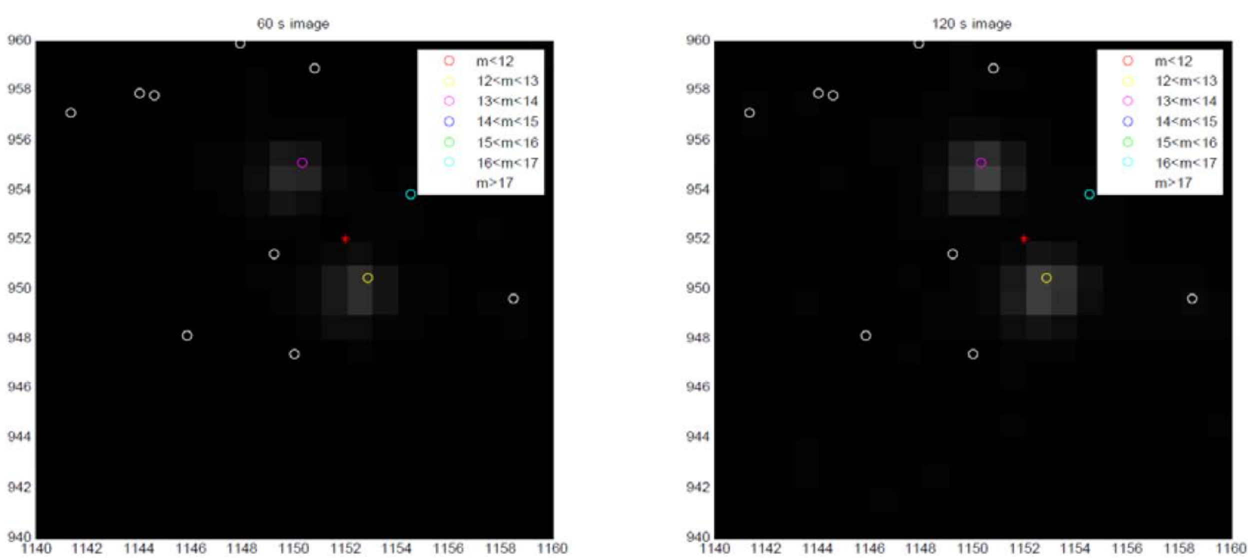

Figure 2. Example of MSM on 60 s and 120 s exposure images (red cross is the centroid).

The filtering and matching techniques above only allow reducing the number of unmatched clusters to a few hundreds, depending on the setting of tuning parameters and thresholds. Most of the remaining clusters are however either SEUs or CCD artifacts. The NAC, being a scientific camera, has an extremely “clean” CCD, only showing a single dark current object of estimated magnitude lower than 16, shown in Figure 3. However, the long exposure times required for early comet detection lead to accumulation of a large number of SEUs, not all of which can be filtered by the size and stretching techniques. On the contrary, shorter integration times on the Navcam lead to few unrecognized SEUs, but the quality of the images is poorer, with a very pronounced dark current pattern which covers the entire CCD and results in artificial clusters of estimated magnitude down to 11. Therefore, to filter SEUs and artifacts, two additional algorithms had to be introduced. First, multiple images taken in the same slot are cross-checked, discarding all clusters which are not always present, i.e. SEU events at specific times. Second, a regularly maintained list of known CCD artifacts for the different cameras is also cross-checked, leading to further filtering of the unmatched clusters. Combining these techniques, only a handful of potential candidates for comet 67P remain, to be visually screened for positive identification.

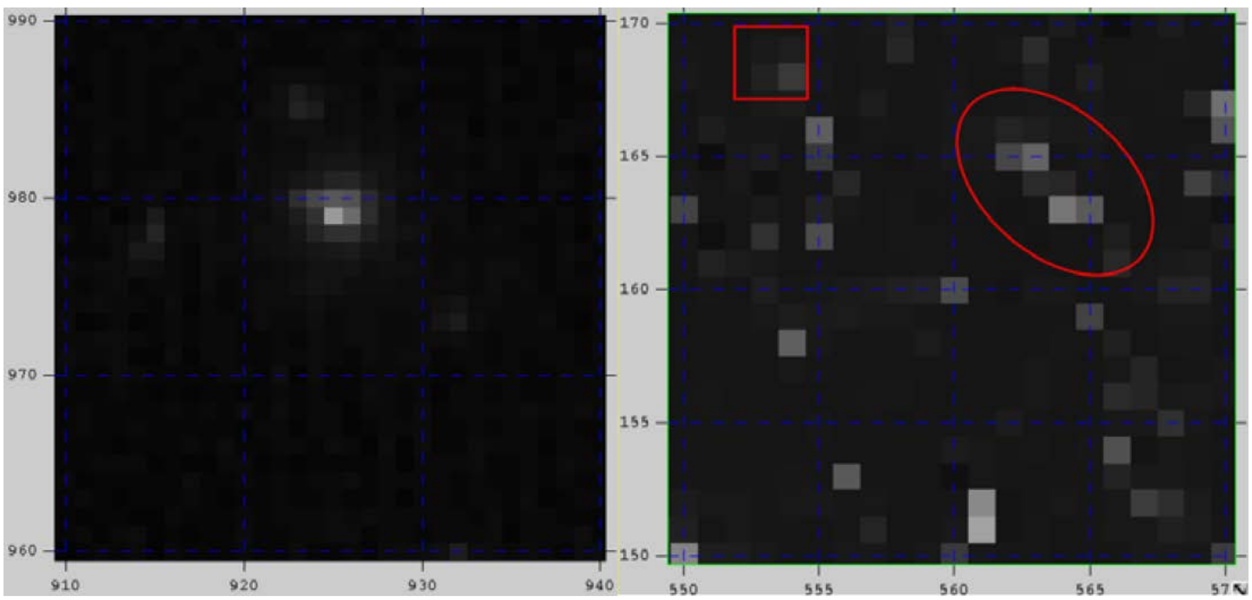

Figure 3. Dark current NAC object (left, estimated visual magnitude V~13.8) and Navcam dark current pattern (right, the square is the brightest star in the area, V~13.0).

For the development and testing of the software, real images taken in 2011 were used. Pointing towards the area of sky in Figure 1, these images exactly matched those to be taken in 2014, with the exception of the presence of the comet. 10 synthetic comets were added to the star field of the NAC and Navcam images used for development, with signals comparable to those which should have been seen in 2014. Results were positive, with all the “fake” comets included in the candidates list. For NAC images, this list included only 2 additional objects: a very large cluster spanning an area of more than 50x80 pixels, which could be identified as the globular cluster M107, and one unidentified object. Although M107 is composed of stars included in the PPMXL catalogue, their proximity results in a single large cluster which cannot be matched. Besides, as it spans a large area on the CCD with very high brightness, M107 would have easily masked the

comet preventing its detection. Nevertheless, this was not considered a critical issue, since M107's position was outside the uncertainty ellipsoids of Figure 1 and the time required for the comet to traverse its extension was less than two weeks. The second unmatched object, with an estimated magnitude of 15.8, was not recognized and could therefore have been a faint asteroid. The list of comet candidates for the Navcam images included instead about 10 unrecognized objects, which could be attributed to faint dark current clusters, not included in the artifacts list.
This provided good confidence that the comet would have been properly detected early with NAC, which indeed happened at the first useful slot. Figure 4 shows part of one of the images where the comet was first identified, with 67P circled besides M107. From the available calibration of the CCD signal to visual magnitude correlation, 67P was estimated to have a visual magnitude of ~13.1 at the time of first detection on the 24th of March, slightly fainter than predicted with the most up to date ground model, but well within the expected uncertainty. The comet was also successfully identified in the first attempted Navcam images on the 8th of May, with estimated visual magnitude of ~10.8, although a larger manual effort would have been required to filter out CCD impurities, had the comet not been previously seen with the NAC.
The comet early detection with the NAC and the subsequent imaging campaign ensured an accurate approach navigation, allowing to steer the Rosetta spacecraft towards its target through optical measurement of the comet centre, which are the subject of the next section.

Figure 4. 67P NAC image from end of March. Credits: ESA © 2014 MPS for OSIRIS-Team MPS/UPD/LAM/IAA/SSO/INTA/UPM/DASP/IDA.

3. Far-approach optical measurements

With comet images available, Rosetta was navigated through a series of 9 braking manoeuvres, spanning from the 21st of May to the 6th of August, from ~1.8 million km to ~100 km from its target. In this whole phase, optical measurements in the form of inertial direction (azimuth and elevation) of the centroid of the comet as seen from the on-board cameras were derived from the imaging data, as input for the orbit determination process. Initially, only NAC measurements were used, followed by a gradual transition to Navcam measurements in May. From the beginning of June, only Navcam data were used, due to restrictions in the availability of Osiris for navigation purposes. Moreover, as described in the introduction, different strategies were followed for the data reduction depending on the apparent size and magnitude of the comet. In particular, until approximately the 3rd of July at ~44000 km of distance, the comet was sufficiently faint to detect enough stars in each image to accurately fit the camera attitude, hence correcting for thermal effects and attitude controller error. Afterwards, when the comet reached an apparent visual magnitude around 2.0 and, coincidentally, a size of around 1 pixel, it was not possible to identify enough stars with the camera integration times set to avoid overexposing 67P. Therefore, for each daily slot of 5 images, the first and the last were taken with longer exposure, with the purpose of assessing the camera alignment close to the images where the comet measurements were taken. Finally, from July 24th it was decided to skip the star images and rely on the known spacecraft attitude and nominal camera alignment for the determination of the comet centre inertial direction. In fact, at a distance of less than 3500 km and with the comet larger than 15-20 pixels, centroiding errors were sensibly exceeding camera attitude errors, thus making star images useless. The same method was used for the first few days of August to provide centre measurements, though with more frequent imaging (1 image per hour instead of 5 per day), in parallel to the beginning of landmark processing activities. Table 1 presents an overview of these different imaging phases. Note that the comet size in pixels is computed assuming a radius of 2 km, and the visual magnitude is the value estimated from the actual images. More details on the comet photometry, including the assessments of comet magnitude and related camera exposure settings are provided in Section 5.

Table 1. Overview of imaging strategy during the comet approach phase

Phase	Dates	D [km]	V_{mag}	Pixels	NAC	Navcam	Images type
1	2014-03-24 2014-05-07	$4.9 \cdot 10^6$ $1.9 \cdot 10^6$	13.1 10.8	0.01 0.02	5 images twice a week	-	Stars + comet in each image
2	2014-05-07 2014-06-06	$1.9 \cdot 10^6$ $378 \cdot 10^3$	10.8 7.2	0.02 0.12	5 images twice a week	5 images per day	Stars + comet in each image
3	2014-06-06 2014-07-03	$378 \cdot 10^3$ 44412	7.2 2.0	0.12 1.03	-	5 images per day	Stars + comet in each image
4	2014-07-03 2014-07-24	44412 3458	2.0 2.0	1.03 13.3	-	5 images per day	Separate star / comet images
5	2014-07-24 2014-08-01	3458 974	2.0 2.0	13.3 47.0	-	5 images per day	Comet only
6	2014-08-01 2014-08-06	974 122	2.0 2.0	47.0 375.6	-	1 image per hour	Comet only

The data reduction process for the generation of optical measurements can be grouped in three macro-steps: 1) the processing of an image to obtain centroid and estimated visual magnitude of each cluster of active pixels, 2) the matching with the stars from the Hipparcos/Tycho catalogue to fit a precise camera attitude, and 3) the conversion of the centroid of the target through such attitude to inertial RA and DE. This process is the same for both cameras, though the tuning of many parameters - as well as the distortion model and magnitude calibration curve to be employed – is different for NAC and Navcam. Moreover, in phase 4 of Table 1, the fit of the camera attitude was done on separate images, and was completely skipped in phases 5 and 6, where the camera attitude knowledge was externally fed to the program to convert centroid information to RA and DE.

More in details, step 1) starts from the cleaning of each image for several effects, such as hot pixels, flat field correction and charge transfer efficiency, with the purpose of improving its quality. Then, the mean background level is determined, and all pixels with an electron content (expressed in Digital Units, DU) at least N times the noise level above the background are flagged as active. Active pixels are clustered together as shown in Figure 5, and the total signal rate (STR) of each clusters in DU/s is evaluated and converted to a visual magnitude, through calibration curves derived from the fit of Sun-like stars to the signal levels seen in calibration images from the different cameras (an example is given in Figure 5 for Navcam-A). The list of clusters is then filtered for several criteria (e.g. minimum number of pixels, minimum signal rate, no saturated pixels) and the centroid is determined for of all objects. The dependency on the centroiding method is not very strong, and a mono-dimensional fit of a Gaussian curve over 5x5 windows was used operationally. The image processing is concluded with the conversion to camera frame of the centroid positions of all clusters, including the application of a camera dependant distortion correction (e.g. for the Navcam, this is 5th order polynomial).

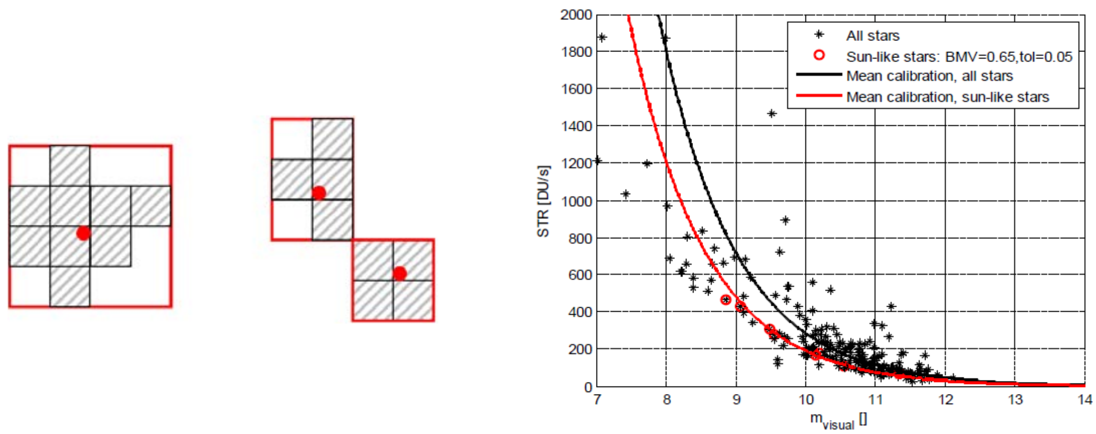

Figure 5. Data reduction process details: pixels clustering and signal-magnitude calibration

Proceeding to step 2), the attitude determination is then performed, using the a-priori knowledge based on star tracker and default alignment as initial guess. Several methods are available, coming from different stages of development of the optical navigation software and different adaptations to the different on-board cameras. The basic concept is however always the same: first, the clusters from step 1) are matched with the stars from the Hipparcos/Tycho catalogue in a given magnitude range. A matching is accepted only when a unique star is found within a given search area (to avoid mismatches in dense star regions), and when the angular distance from the cluster centroid is below a given threshold. Then, based on these stars, an estimation of the camera attitude is performed. This is done either through a standard q-Method iterated until the maximum residuals of all star directions is below a convergence criterion, or through a more complex weighted least square process known as gnomonic projection, or through the successive application of both to achieve a better accuracy. All these algorithms require a relatively large number of thresholds and parameters to execute. Whereas some were fixed to values which were shown to provide good performances, others were adapted throughout the approach to the current conditions for an optimum performance. For instance, the maximum residual on any star for the convergence of the q-Method was set to one NAC/Navcam pixel, but the magnitude range for the

Hypparcos/Tycho stars was varied depending on the exposure times, and hence on the range of stars visible in the images.

From the application of the above methods, the camera attitude at the time of the image is known with a good precision, with RMS of the residuals which depend on the threshold settings but can be reduced to less than 1/10 of a pixel. Step 3) mentioned above, then simply consists in the identification of the cluster in the expected direction corresponding to the target, and the conversion of its camera frame centroid to inertial RA and DE, on the basis of the obtained attitude fit. Note that the final inertial measurements are corrected for stellar aberration, whereas the light time is not applied since is already considered in the orbit determination software.

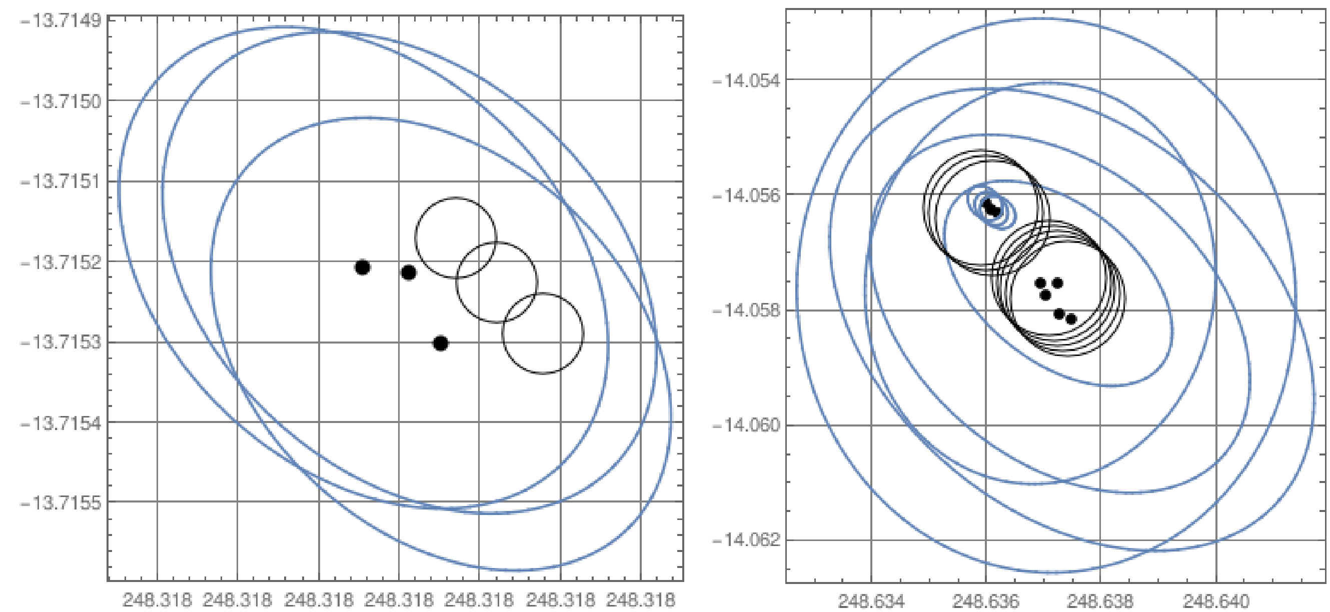

Figure 6. Comet centre measurements during approach phases 1 and 2 (x=RA, y=DE, deg)

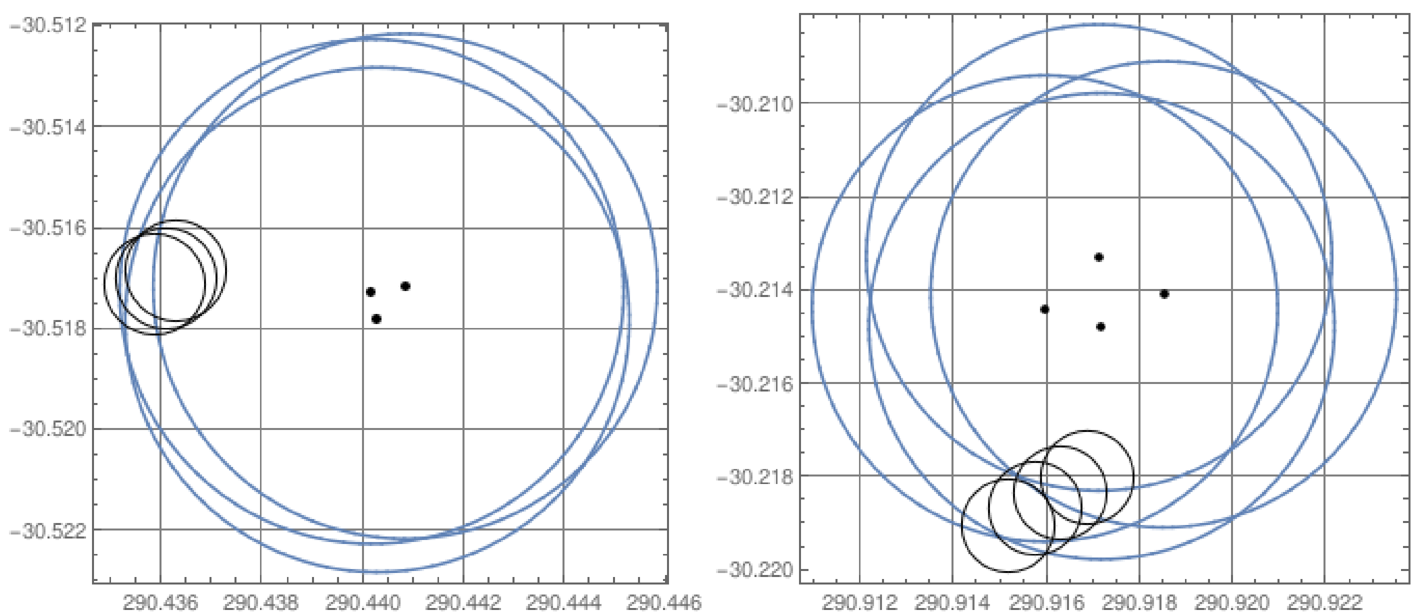

Figure 7. Comet centre measurements during approach phases 3 and 4 (x=RA, y=DE, deg)

The orbit determination results for Rosetta's approach to 67P, which provide the most reliable assessment of the accuracy of the optical measurements, are presented in a separate paper ([8]). Here however, Figure 6 and Figure 7 aim at giving an impression of the quality of such data. All graphs present inertial RA and DE of 67P as seen from Rosetta. Black dots represent the measurements (NAC or Navcam), with the assigned uncertainty ellipsoids in blue. The black circles instead represent the inertial directions derived from the final reconstruction of the orbits of Rosetta and 67P, which therefore merges optical and radiometric information. By comparing the spread of the optical measurements with the actual trajectory (and especially the shift between one image and the next), it is possible to qualitatively assess the measurements noise for the two cameras and for the different phases of the approach. The 3 data points from phase 1 (Fig. 6 left) are from the NAC, and show a very small spread of the observations, limited to ~0.1 mdeg. The points for phase 2 (Fig. 6 right), including both NAC and Navcam, show a much larger dispersion of the 5 Navcam data points, which is consistent with the worse pixel resolution (5 mdeg instead of 1 mdeg). The data of phase 4 (Fig. 7 left) prove instead the good quality of the approach with separate comet and star images with the Navcam. In fact, even though the luminosity of the comet was preventing from directly fitting an attitude for consistent data reduction, the averaging of the camera alignments before and after the comet images allowed achieving accuracies in the order of 1 pixel. In particular, it was assessed that the Navcam alignment as reconstructed from the images had a constant bias of about (0.8, 2.5) pixels in (X,Y) with respect to the values used on-board, with an additional noise from image to image which could reach up to ± 1 pixels on both axes. The constant bias was commanded on-board in the beginning of August, with the purpose of improving the measurements quality for the upcoming landmark processing. Finally, the data of phase 5 (Fig. 7 right) show an even larger dispersion of the measurements, corresponding to the period when the comet started to appear as a largely extended object, with errors in the order of up to 5 pixels. This was however limited to a very brief period in time, as landmark-based optical navigation was started as soon as the comet reached around 300 pixels of size, as described in [3].

4. 67P rotational period light curve estimation

In parallel to the final stages of the far-approach optical navigation, and prior to the onset of the landmark-based optical navigation (see references [2] and [3]), it was paramount to have an initial guess of the rotational period of 67P. This period was used as input for the image-stitching process, leading towards an initial attitude reconstruction of 67P. The photometric data for this lightcurve was obtained trough the so-called "asteroid-tracking" mode of the NavCam.

The asteroid tracking mode processes a sub-window of a single CCD-frame returning the overall mean geometrical and photometric position of the sub-window, as well as total magnitude, total accumulated signal and total target pixels. From this data, it was possible to recompute the signal strength of target in the CCD's subwindow. Such processing was commanded to be done every 2.5 s during a period of 18 days starting on 2014/07/13. This date was chosen as the apparent diameter of 67P was expected to be well above 1 pix on the NavCam's CCD (4.35 pix for a 2.5km radius of 67P). The asteroid tracking was not performed continuously, but contained gaps needed for standard flight-dynamics maintenance operations such as wheel-off-loadings, two of the four far-approach trajectory manoeuvres (FAT3 and FAT4) and imagery needed for the far-approach optical navigation as described in section 3. To this end, five time-blocks were identified where tracking data was taken :

ID	Start Time (TDB)	End Time (TDB)	Info
1	2014/07/13T07:48:09	2014/07/16T06:05:07	97955 frames
FAT3	*2014/07/16T11:15:03*	*2014/07/16T11:40:00*	*ΔV = 10.967 km/s*
2	2014/07/16T23:22:09	2014/07/18T07:10:07	141802 frames
	2014/07/20T07:12:09	2014/07/23T03:00:07	
FAT4	*2014/07/23T10:39:23*	*2014/07/23T10:55:57*	*ΔV = 4.823 m/s*
3	2014/07/23T03:00:07	2014/07/25T06:34:07	134975 frames
	2014/07/29T10:07:23	2014/08/01T09:48:21	

The 3 main data-blocks taken and the location of the FAT3 and FAT4 manoeuvres as a reference.

Modelling the lightcurve of a continuously rotating object is, in essence straightforward by fitting various Fourier components to the lightcurve $S(t)$ as :

$$S(t) = S_0 + \sum_{n=0}^{N} a_n \cos\left(\frac{2\,\pi\,n\,t}{T}\right) + b_n \sin\left(\frac{2\,\pi\,n\,t}{T}\right),$$

with T the signal's period, a_n and b_n the Fourier components and N the maximum order. This is true when the distance between camera and target is static. In the case of Rosetta and 67P, the distance is not static and a distance correction needs to be applied to the signal. The measured flux stemming from 67P is therefore inverse proportional to the distance squared :

$$F(t) = \frac{S(t)}{(d + vt)^2},$$

where d and v represents the distance, respectively velocity at a reference time t_{ref} and t the time since this $t_{ref.}$ However, as Rosetta was not flying in a direct line towards 67P, the distance needed to be compensated for the impact parameter. The incoming flux can thus be written as :

$$F(t) = \frac{S(t)}{d^2 + 2\,v\,d\,t\cos(\varphi) + v^2 t^2} + o,$$

with φ the angle between the velocity vector of Rosetta and the target vector. The factor o is added as an offset to compensate for any instrumental bias. A final correction could be applied representing the tracking correction to the phase-angles of the Fourier components. However, the latter would only be valid if the axis-of-rotation of 67P was perpendicular to the orbital plane of Rosetta.

In combination to the correction for the impact parameter, a phase angle correction needed to be applied to the signal. This used phase function was, at the time of measurements, taken to be

$$P\big(\alpha(t)\big) = (1 - G)\exp\left\{-3.33\ \tan\left(\frac{\alpha(t)}{2}\right)^{0.63}\right\} + G\exp\left\{-1.87\ \tan\left(\frac{\alpha(t)}{2}\right)^{1.22}\right\},$$

with $\alpha(t)$ the sun-target-spacecraft angle as function of time, and G set to 0.11 (See [11]). This correction was applied to the data itself and the corresponding errors.

Assuming the set S=$\{\{t_i, s_i, w_i\}: i \in [1, M]\}$ represents the measured lightcurve data s_i measured at time t_i in analogue digital units (ADU) with the photon noise taken as weight $w_i = \sqrt{s_i}$. Furthermore, in the next part, we assume $S_0 = 1$, removing the extra degree of freedom we have. The signal strength will therefore be absorbed by the parameters d and v which will loose their physical meaning. Fitting the data was done in several steps:

1. Correct the data set with the with the phase-function:
$$S \rightarrow S' = \{\{t_i, s'_i, w'_i\}: i \in [1, M]\} = \left\{\left\{t_i, \frac{s_i}{P(\alpha(t_i))}, \frac{w_i}{P(\alpha(t_i))}\right\}: i \in [1, M]\right\}$$
2. Fit $d + vt$ to the inverse square root of the signal to get a first estimate of the parameters d and v.
3. Fit the earlier defined function $F(t)$ to the signal, using the least-squared method making use of the values obtained in step 2. The total number of Fourier components used was 12.
4. Clean-up of the signal from any cosmic rays and other SEU's by removing all data points which are more then 5σ deviating from the fit in step 3.
5. Repeat 3 and 4 to obtain the final result.

As the total dataset was divided by the two FAT manoeuvres, altering the orbital plain and, more importantly, the relative velocity of 67P with respect to Rosetta. Three separate fits were performed of the data., leading to the following period estimates :

ID	**Start Time (TDB)**	**End Time (TDB)**	***T (h)***
1	2014/07/13T07:48:09	2014/07/16T06:05:07	12.4394 ± 0.0002
2	2014/07/16T23:22:09	2014/07/23T03:00:07	12.4273 ± 0.0001
3	2014/07/23T03:00:07	2014/08/01T09:48:21	12.4125 ± 0.0001

The results of these fits are visualized in Figure 8. As the results of the 3 datasets are more-or-less similar (up to 1min), we decided that an estimated period of 12.426 ± 0.013 h would suffice as input for the initial attitude reconstruction. The differences of the outcome could be attributed to the 2 FAT manoeuvres, which in time aligned Rosetta better with 67P, improving its estimate. Furthermore, it must be mentioned that these estimates are measured in space-craft frame and do not correct for the change in attitude of Rosetta.

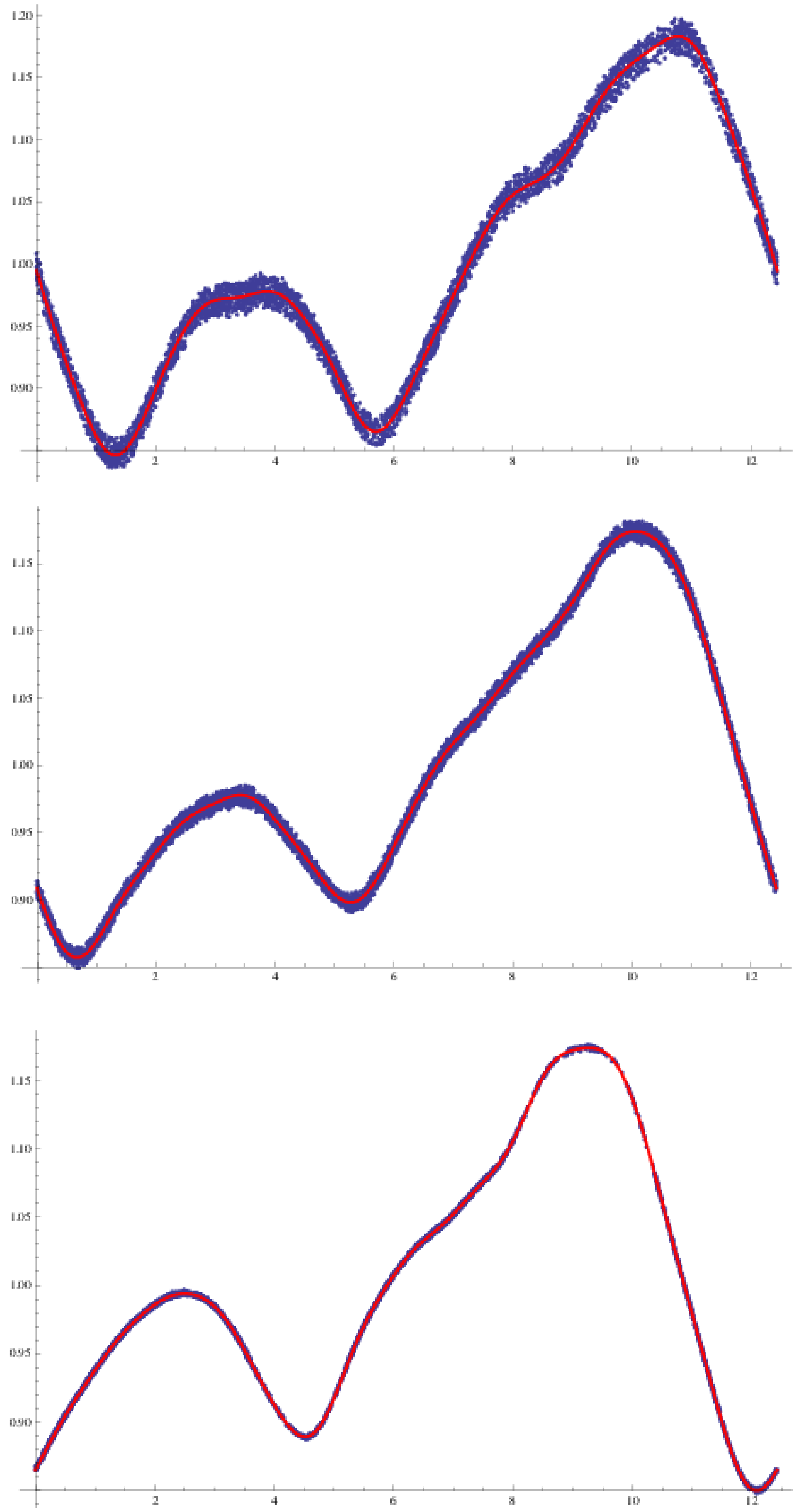

Figure 8. Periodically folded linearised lightcurves and their corresponding fit. Top to bottom, the 3 separate datasets (ID 1, ID2 and ID3). The redline is the fitted signal *S(t)*.

5. Operational photometric analysis of comet 67P

Although more detailed studies are left to the science teams, a basic analysis of the photometric properties of 67P was carried out operationally throughout the approach and the characterization phases of the mission, with the purposes of supporting camera exposure times definition and automatic landmark processing through maplets.

During the approach phase, until the comet extended larger than a pixel in the beginning of July, a simple H-G magnitude model from Lowry [9] was used as reference for the definition of both Navcam and NAC exposure times. For the NAC, the operational strategy involving the Osiris team required Flight Dynamics to fix the exposure of all approach images already before comet detection. Therefore, it was decided to span a very large range of exposure times in the 5 images of each Osiris navigation slot. In particular, a span of $\pm 4\sigma$ was taken on the magnitude model (± 1.5 mag) and of $\pm 3\sigma$ for the magnitude-signal calibration curve to define a range of exposures at the time of each imaging slot, assuming 50% of the saturation (2^{16} bits) as target image level. This resulted in exposure times from 60 to 720 s on March 24th, and from 1.6 to 67 s on June 4th. Navcam exposures could instead be tuned at short term planning level, therefore allowing for smaller margins to be taken, based on the empirical data from the previous images. A posteriori analysis of the reconstructed magnitude from each navigation slot, shown in Figure 9, showed that the comet was consistently slightly fainter (0.2-0.5 magnitude) with respect to the Lowry model, except for an outburst of activity from 67P in late April - which gradually faded away in the following days - and an overall slight increase in luminosity just before reaching the pixel size, at an apparent magnitude ~2.0.

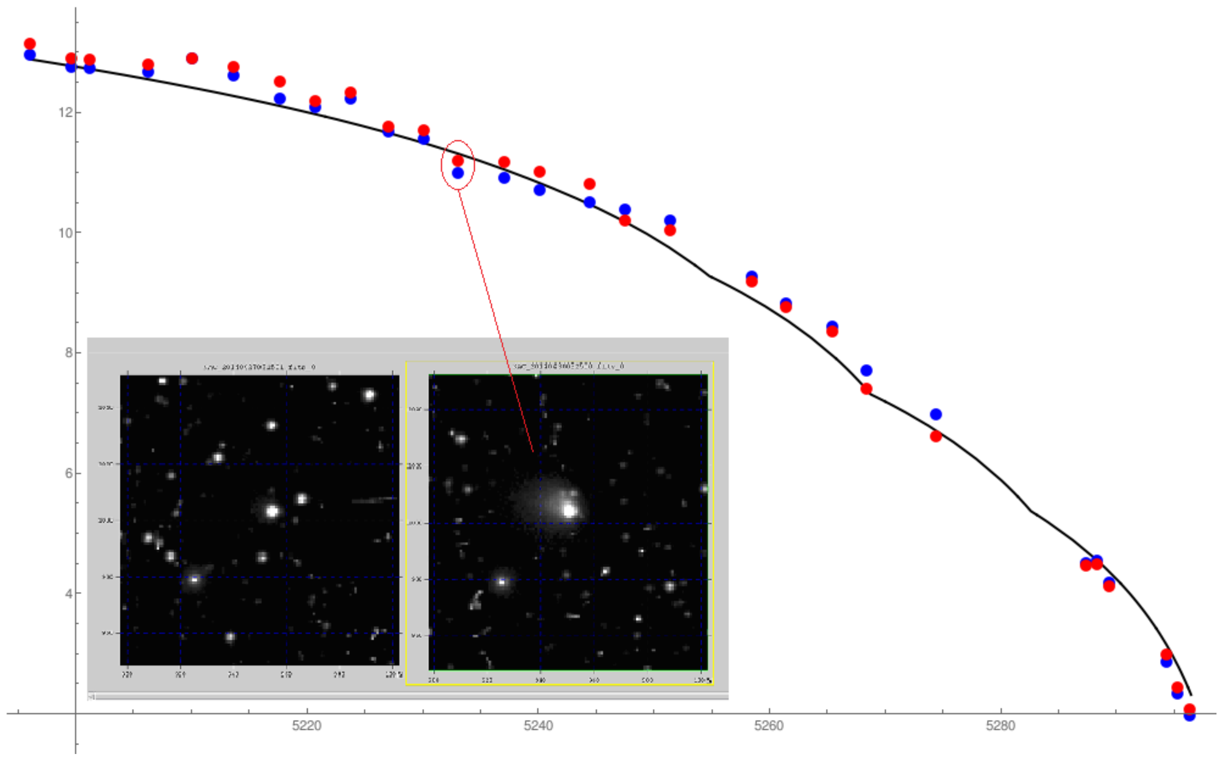

Figure 9. Comet visual magnitude 24th March - 2nd July: comparison of Lowry H-G model and actual magnitudes from Navcam/NAC images (red-blue: estimate range in each slot).

At comet arrival in beginning of August, two main photometry-related activities were initiated. On one side, the navcam integration times were manually defined at short term planning level (twice per week) on the basis of the brightness in the previous images. A maximum value of ~3000 DU over the full comet body was targeted, in order to avoid saturation (2^{12}=4096 DU). Over the course of the full characterization of 67P (August to November), a wide range of phase angles was covered, at sun distances from ~3.6 to ~2.8. This allowed building an empirical table model for the exposure time as a function of the phase angle, normalized at 1 AU Sun distance, as shown in Table 2.

Table 1. Navcam exposure empirical model (α_{min}, α_{max} in deg, t_{exp} in s @ 1 AU)

α_{min}	10	16	24	28	38	52	60	68	80	88	92	100	110
α_{min}	16	24	28	38	52	60	68	80	88	92	100	110	120
t_{exp}	0.08	0.10	0.14	0.17	0.23	0.27	0.31	0.37	0.48	0.52	0.61	0.72	0.83

In parallel, a theoretical photometric model was implemented, allowing to determine the expected pixel signal value in DU given the geometry (phase angle α, observation emission angle e, Sun incidence angle i), the Sun distance d_{Sun}, the albedo of the surface a, and the characteristics of the camera and its filter condensed in the parameter $k_{cam,filt}$. This model was to be used for a variety of purposes, such as simulation of future images for operations preparations, automatic calculation of the exposure times in alternative to the empirical model, and as core mathematical formulation for the maplets methodology, which was to be gradually transitioned into operations for the identification of landmarks, as described in [3].

A vast number of photometric models were available in literature, and an analysis of the most common was carried out to assess the most suitable for comet 67P, by fitting the free parameters to the images that were continuously being taken for navigation purposes. Although the selection of the model type and an initial tuning of the parameters were already available in early September, so that the maplets could be phased into operational usage in parallel to manual processing for the generation of landmark observations, the results presented here correspond to the final analysis, which makes use of all available images until the end of 2014. These span all phase angles from 10 to 120 deg, summing up to ~4400 images and allowing for very detailed scan of the phase angle dependency of 67P's photometric properties.

A modified version of the Lunar reflectance model developed by McEwen ([10]) was finally selected, which is reported in Equation (1). The original lunar model combines the isotropic diffusive reflectance model from Lambert (R_L) and the single scattering reflectance model from Lommel-Seeliger (R_{LS}) through a weighting function $L(\alpha)$. Since $L(\alpha)$ is an exponential of the phase angle, the model describes an object with purely Lambert behaviour at the sub-solar point and gradually approaching the Lommel-Seeliger behaviour with growing phase angles. Since the nominal Lunar model alone is unable to fit the photometric data from 67P with a constant albedo, the additional term $P(\alpha)$ multiplying the full reflectance function was added, to account for the phase angle dependency in the CCD signal measurements. This addition allowed to drastically improve the fit.

Modified Lunar model	Model parameters	Exposure time calculation	
$S = \Lambda \cdot a \cdot R + \Phi$			
$\Lambda = \dfrac{K_0 \cdot t_{int} \cdot K_{cam,filter}}{{d_{Sun}}^2}$	$\Phi = 350\ DUs$		
$R = P \cdot [(1-L) \cdot R_L + L \cdot R_{L-S}]$	$\beta_0 = 0.4966\ rad$	$a_{MAX} = \sim 1.3$	
$R_L = Cos(i)$	$\alpha_0 = 1.0472\ rad$	$R_{MAX} = P \cdot [(1-L) \cdot Sin(\alpha) + L]$	(1)
$R_{L-S} = \dfrac{Cos(i)}{Cos(i) + Cos(e)}$	$K_0 = 47.8312\ \dfrac{AU^2 \cdot m^2 \cdot sr}{W \cdot s}$	$t_{int} = \dfrac{(S_{target} - \Phi) \cdot {d_{Sun}}^2}{K_0 \cdot K_{cam,filter} \cdot a_{MAX} \cdot R_{MAX}}$	
$P = e^{-\frac{\alpha}{\beta_0}}$	$K_{cam,filter}\ [\dfrac{\mathrm{DU.m2.sr}}{\mathrm{W}}]$		
$L = e^{-\frac{\alpha}{\alpha_0}}$			

The resulting parameters for the modified lunar model are: the camera constant $K_{cam,filter}$ defined by the camera supplier; the background level Φ, which was fixed to 350 DUs as an average of the available images, and the free coefficients α_0 tuning the $L(\alpha)$ weighting function, β_0 tuning the additional $P(\alpha)$ phase dependency, and K_0 as a constant scaling parameter. Note that the albedo has always been arbitrarily set to 1, using K_0 to also absorb the actual physical albedos of the comet. Figure 10 shows the empirical values obtained for the weighting function $L(\alpha)$. Due to the large dispersion of the data, which only roughly follow an exponential trend, it was decided not to calibrate α_0, keeping the value from the original formulation by McEwen. The decision to use an exponential fit for the additional term $P(\alpha)$, as well as the calibration of its coefficient β_0 and of the scaling K_0, was instead taken on the basis of the data in Figure 11, where the residual term $P(\alpha){\cdot}K_0$ is plotted. In order to produce that graph, $P(\alpha){\cdot}K_0$ was estimated - for all available images - for each of the facets of a 250k facets shape model built with several techniques, as described in [3]. A different value of $P(\alpha){\cdot}K_0$ was obtained for the Lambert, Lommel-Seeliger, and Lunar models, and the mean and standard deviations for each image were then computed.

The dispersion of the different models is similar, with a slightly better agreement of the Lunar model with respect to an exponential fit. Other analytical models like Hapke's are more complex but did not fit the empirical data better and there fore the exponential law was kept.

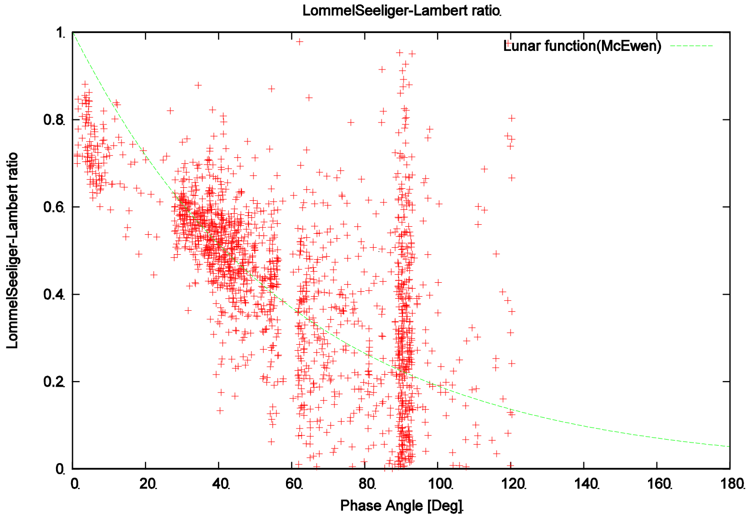

Figure 10: Empirical values of $L(\alpha)$.

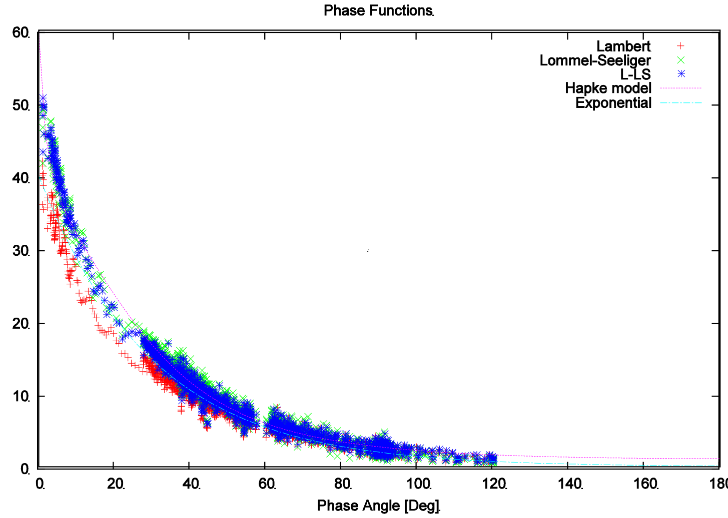

Figure 11: Empirical values of $P(\alpha)\cdot K_0$.

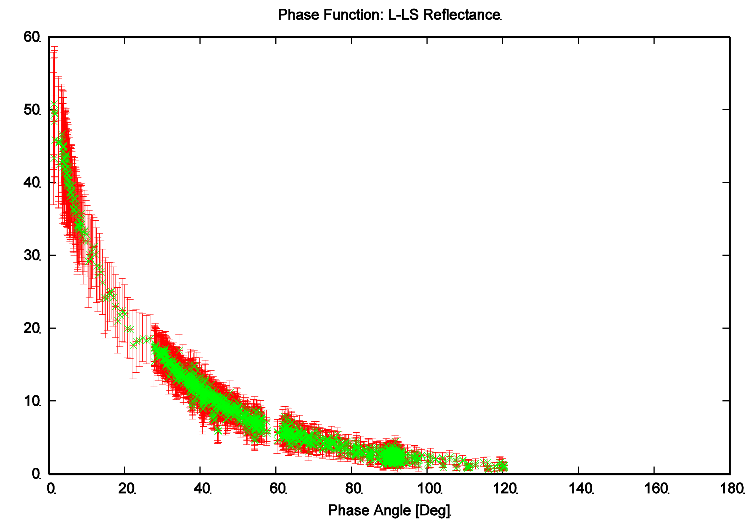

Figure 12: Empirical values of $P(\alpha)\cdot K_0$ with the related 1σ uncertainties from the shape model facets.

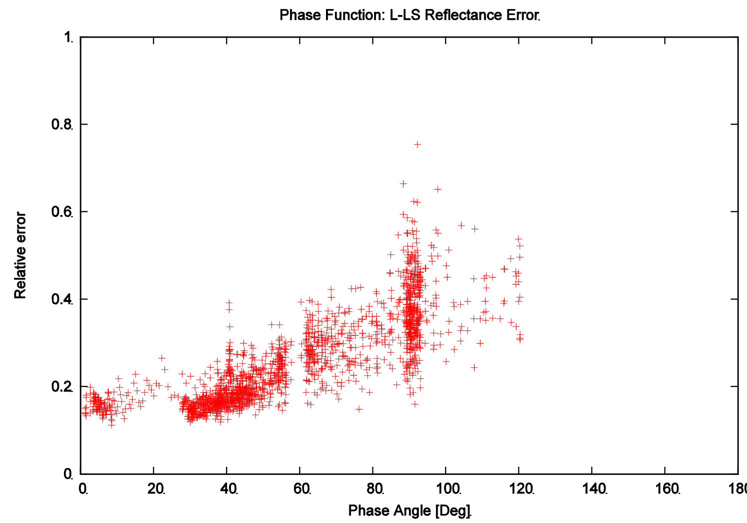

Figure 13: Ratio of error with respect to the exponential fit of $P(\alpha)\cdot K_0$ and 1σ uncertainty.

Focusing on the Lunar model, Figure 12 and Figure 13 show the 1σ standard deviation band for all images and the error between the experimental data and the final $P(\alpha)\cdot K_0$ fit divided by 1σ. This shows how the agreement of the final model with the data is sensibly better at lower phase angles, with a degraded accuracy above 60 deg, confirming other literature results.
Although the model was directly used as defined in Equation (1) for the maplet application, it could not be directly applied to exposure times generation. In fact, these have to be tuned for the maximum signal value expected in an image, whereas the fit for the maplets is obtained as an average over the full shape model. The inverse formula for the exposure time calculation is also shown in Equation (1), and is based on an analytical evaluation of the maximum of $R(\alpha, e, i)$

over emission and incidence, which corresponds to a point in the mirror meridian in between the limb and the sub-solar point. However, Figure 14 proves that this is not an accurate representation of the maximum expected pixel value, since the blue curve plotted with the parameters determined for the maplets (Equation 1), clearly does not fit well the integration times defined empirically as described in the beginning of the section. A plausible explanation is that the reflectance model is outside its range of applicability at those high emission angles. As a consequence, the same model was directly fit to the exposure times, obtaining a much better fit in the green curve, with $\beta_0=0.76024$ and $K_0=31.291$.

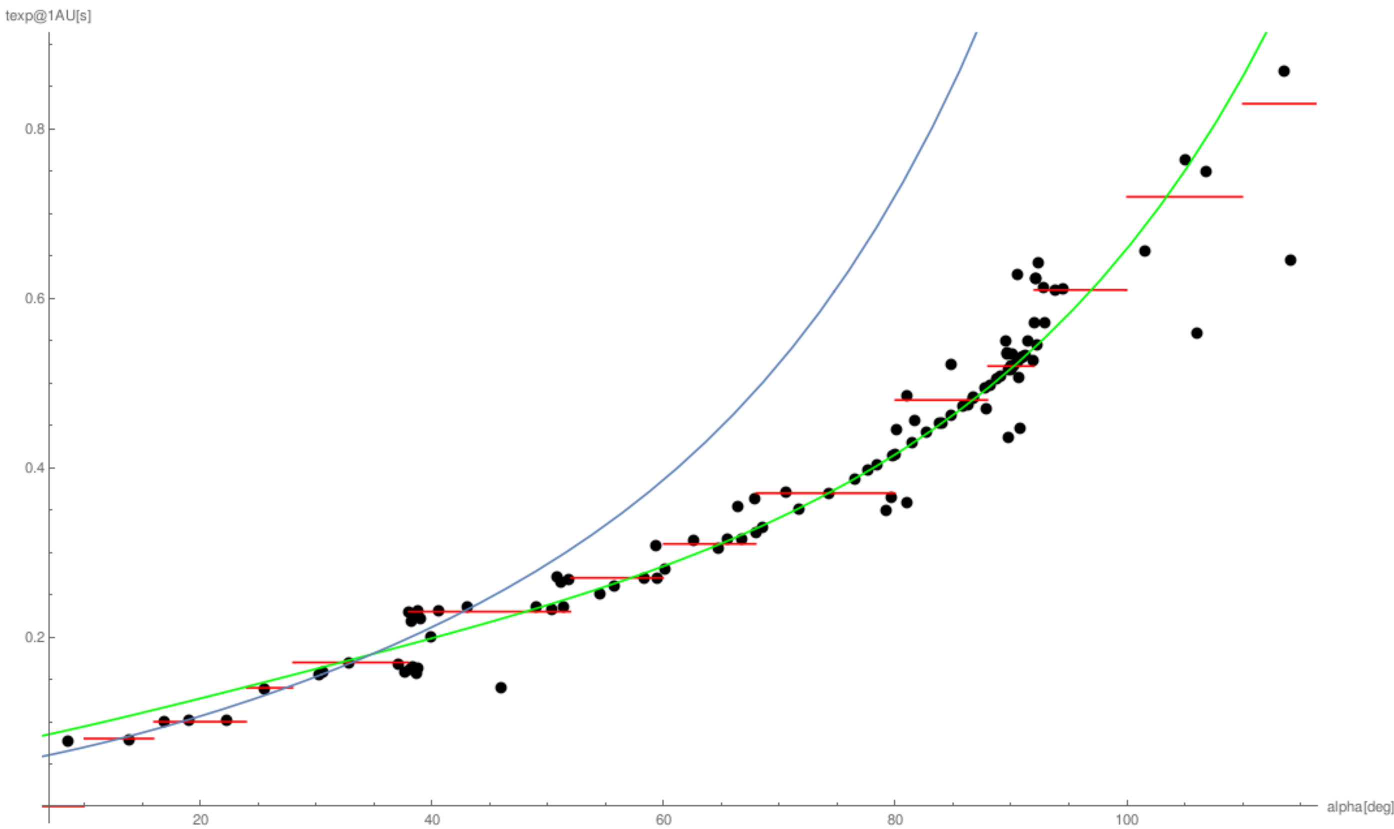

Figure 14: Navcam exposure at 1 AU vs. phase angle: experimental data (black), empirical model (red), modified Lunar model exposure times fit (green) and maplets fit (blue).

The modified Lunar photometric model with these final parameters values were implemented in a tool which now allows automatic computation of the integration times for each new image. By setting a target level of 3000 DU, all images acquired with such method in the past 8 months at comet distances between 100 and 400 km and phase angles between 60 and 120 deg show a good agreement with predictions, with brightest pixels conservatively in the order of 2700-2800 DUs.

6. Conclusions

In the frame of ESA's Rosetta mission, this paper presents an overview of the optical data processing which allowed to successfully detect Rosetta's target 67P/Churyumov-Gerasimenko, navigate the spacecraft through target centroid information until achieving the first ever rendez-vous with a comet, and study the comet photometry for the purpose of maplets tuning and camera exposure time calculation.

Details of all developed methods as well as quantitative results from operational data were provided. The algorithms for comet detection with the scientific Osiris NAC ensured positive identification at the first attempted slot, when the comet had an estimated visual magnitude of ~13.1. In the following months, orbit determination activities were based on the merging of radiometric data with optical measurements of the centre of the comet. The data reduction process described in the paper allowed deriving the inertial direction of 67P with an accuracy which was assessed to be down to 1/10 of a pixel until when enough stars could be found for attitude fitting, and around 1 pixel when averaging of the alignment in two dedicated star images was necessary for this purpose. Finally, detailed studies on the photometric properties of 67P allowed to produce a modified Lunar reflectance model which is sufficiently accurate for both maplets processing and automatic calculation of the camera exposure times, ensuring a smooth transition from heavy manual optical processing to a nearly automatic system, which is routinely used today for the continuation of the Rosetta mission.

7. References

[1] Budnik F., Companys V., Lauer M., Fertig J., Morley T., Godard B., Munoz P., Casas C., and Janarthanan V., "Rosetta: Comet Approach and Proximity Navigation", Proceedings of 25th International Symposium on Space Flight Dynamics (ISSFD), Munich, Germany, October 2015.

[2] Antal-Wokes D.S., Castellini F. and Kielbassa S., "Rosetta: Imaging Tools, Practical Challenges and Evolution of Optical Navigation Around a Comet", Proceedings of the Astrodynamics Specialists Conference – ASC, August 2015, Vail, CO, United States.

[3] Pardo de Santayana R., and Lauer M., "Optical Measurements For Rosetta Navigation Near The Comet", Proceedings of the 25th International Symposium on Space Flight Dynamics (ISSFD), Munich, Germany, October 2015.

[4] Keller H. U., et al., "OSIRIS The Scientific Camera System Onboard Rosetta", Space Science Reviews, Volume 128, Issue 1-4, pp. 433-506, 2007.

[5] Lauer M., Herfort U., Hocken D., and Kielbassa S., "Optical Measurements for the Fly-By Navigation of Rosetta at Asteroid Steins", Proceedings of the 21st International Symposium on Space Flight Dynamics (ISSFD), Toulouse, France, October 2009.

[6] Pardo de Santayana R., Lauer M., Muñoz P., and Castellini F., "Surface Characterization And Optical Navigation At The Rosetta Flyby Of Asteroid Lutetia", Proceedings of the 24th International Symposium on Space Flight Dynamics (ISSFD), Laurel, MD, May 2014.

[7] Roeser S., Demleitner M., and Schilbach E., "The PPMXL Catalog of Positions and Proper Motions on the ICRS. Combining USNO-B1.0 and 2MASS", The Astronomical Journal, Vol. 139, No. 6, April 2010.

[8] Morley T., Budnik F., Godard B., Muñoz P., and Janarthanan V., "Rosetta Navigation from reactivation until arrival at comet 67P/Churyumov-Gerasimenko" , Proceedings of the 25th International Symposium on Space Flight Dynamics (ISSFD), Munich, Germany, October 2015.

[9] Lowry S., et al., "The nucleus of Comet 67P/Churyumov-Gerasimenko", Astronomy and Astrophysics, Vol. 548, December 2012.

[10] McEwen A.J., "A precise Lunar Photometric Function", 27th Lunar and Planetary Conference, pp. 841-842, 1996.

[11] Dymock R., "The H and G magnitude system for asteroids", Journal of British Astronomical Association", vol. 117, pp. 342—343, 2007